Unique stiffness-deformability features of dendrimeric silica reinforced HDPE nanocomposites obtained by an innovative route

Duarte Cecílio, Maria Cerrada, Ernesto Pérez, Auguste Fernandes, João Paulo Lourenço, Timothy F.L. Mckenna, M. Rosário Ribeiro

Unique stiffness-deformability features of dendrimeric silica reinforced HDPE nanocomposites obtained by an innovative route

Duarte M. Cecílio[a], Maria. L. Cerrada[b]*, Ernesto Pérez[b], Auguste Fernandes[a], João Paulo Lourenço[a,b], Timothy F.L. McKenna[d] and M. Rosário Ribeiro[a]*

[a]Centro de Química Estrutural and Departamento de Engenharia Química, Instituto Superior Técnico, Universidade de Lisboa, Av. Rovisco Pais 1, 1049-001 Lisboa, Portugal,

[b]Instituto de Ciencia y Tecnología de Polímeros (ICTP-CSIC), Juan de la Cierva 3, 28006 Madrid, Spain

[c]Departamento de Química e Farmácia, Faculdade de Ciências e Tecnologia, Universidade do Algarve, Campus de Gambelas, 8005-139 Faro, Portugal

[d]Université de Lyon, CPE Lyon, CNRS, UMR 5128 - Catalyse, Polymérisation, Procédés et Matériaux (CP2M), Bat 308F, 43 Blvddu 11 Novembre 1918, 69616 Villeurbanne, France

*E-mail addresses of corresponding authors:

rosario@tecnico.ulisboa.pt (M. Rosário Ribeiro); mlcerrada@ictp.csic.es (M. L. Cerrada)

Abstract

A set of dendrimeric silica (DS) reinforced polyethylene-based nanocomposites is prepared using a novel and straightforward *in-situ* catalyst supporting procedure by means of "*in-situ*" polymerization technique, labeled DS-SA. These materials are characterized with regard to molar masses, filler dispersion, thermal stability, crystalline characteristics, thermal properties and mechanical response and then compared with an equivalent set of samples prepared using a more common method, named DS-MAO, as well as a non-reinforced HDPE reference. The mechanical performance of all these materials is discussed based on the crystalline features and molar masses of the polymeric component together with the dispersion of the DS nanofiller. The results of this study confirm the potential of the DS-SA approach as an innovative and promising technique, with resulting materials achieving superior filler dispersion and significantly higher mechanical performance compared to their DS-MAO analogues at high filler loadings, while retaining the limit stretching ability of HDPE.

Keywords: Nanocomposites, Dendrimeric silica, *In-situ* catalyst supporting, Polyethylene, Mechanical response

1. Introduction

Composite materials consisting of a hybrid organic matrix and inorganic filler components exhibit interesting properties that allow their use for a wide variety of applications. The incorporation of an inorganic constituent into a polymeric matrix, such as polyolefins, which are the most widely manufactured and consumed polymers in the world, might lead to a reinforcement effect that yields marked improvements to the mechanical, thermal, biocidal, dielectric and magnetic properties, depending on the specific characteristics of the inorganic component, with regard to those exhibited by the pristine polymer [1–6].

The inorganic component might have dramatically different effects depending not only on its nature but also on its particle size. Most of the initial research conducted on these types of composites employed micron-sized inorganic fillers [7–11]. However, incorporation of nanomaterials has been proved as promising approach to further improve the performance of the resulting nanocomposites [12]. A significant increase in interfacial area between the polymeric matrix and the filler is achieved if the size of the latest is nanometric instead of micrometric. This enlargement can promote a more suitable compatibilization and, consequently, a higher reinforcement effect. Accordingly, an effective reduction in the necessary filler content can be achieved for reaching a specific reinforcement degree [13] provided that a uniform dispersion of the nanoparticles can be ensured [14,15].

In this context, mesoporous silicas are a promising choice as fillers due to a resilient structure, which can resist the forces exerted by the polymer attempting to separate the two components. Moreover, mesoporous silica particles present enhanced surface area and, thus, a higher reinforcement potential. By far, the MCM-41 and SBA-15 types [11,12,16,17] have been the most popular mesoporous silicas employed up to now.

In-situ polymerization is a recognized approach for the incorporation of inorganic (nano)particles into polymers [1]. If silica (nano)particles are used as fillers, they can be modified with appropriate compounds in order to improve their additional bonding or physical interactions with the monomer prior the final polymer is synthesized. Alternatively, the

monomer can be copolymerized with a polar comonomer in order to increase the compatibility with the hydrophilic silica surface [19,20]. Compared with the direct processing, (mixing the inorganic filler with either molten polymer or polymeric solution) *in-situ* polymerization might lead to a better dispersion of the (nano)filler as well as better compatibility at interfaces, especially at high (nano)filler contents, turning out in superior reinforcement effects [18,21,22].

Dendrimer-like silica (DS) nanospheres have been recently used as a support for a metallocene catalyst for ethylene polymerization [23]. Its high surface area and unique porosity promote conditions of great accessibility to the silica surface of the catalyst and other reactants. This silica support showed promising results when compared to MCM-41, a more common type of mesoporous silica.

Very recently, we developed an innovative methodology (DS-SA) for the preparation of high-performance polyolefin-based materials. In this approach the MAO is first supported on the DS particles, giving rise to a DS supported MAO activator, which is mixed directly with the metallocene catalyst inside the polymerization reactor. The polymerization of ethylene is then promoted by this *in-situ* supported catalyst, without the need for further external MAO addition. The DS particles play a fundamental role in this approach and are used in a double purpose, for the preparation of the DS supported activator and as a filler. The proposed methodology demonstrated a remarkable catalytic performance, comparable to the reference homogeneous catalyst and, much higher than the one observed for a more common applied catalyst supported polymerization process, (DS-MAO) which consists in a two-step catalyst immobilization process followed by ethylene polymerization promoted by this supported catalyst in the presence of an additional amount of MAO. Moreover, a preliminary evaluation of morphological and crystalline features of polyethylene-based materials highlighted the versatility and ability of the DS-SA method in tailoring polymer properties [24].

This work aims to further investigate the potential of this methodology for the preparation of high-performance HDPE nanocomposite materials namely, in what concerns its ability to improve phase compatibility and dispersion of filler nanoparticles, as well as to assess their final properties and to investigate how the synthetic procedure used can impact them. Thus, several polyethylene-based nanocomposites with different weight contents in DS nanoparticles were prepared by the two aforementioned methodologies and their microstructural details, morphological features, crystalline characteristics, phase transitions and mechanical properties are investigated. A neat polyethylene, obtained by homogeneous polymerization using the same zirconocene catalyst, is used as a reference for the nanocomposites prepared via the two methodologies.

2. Experimental Section

2.1. Materials

Synthesis of the mesoporous materials required tetraethyl orthosilicate (TEOS, 99%, Aldrich) as silicon precursor. 1-hexadecylpyridinium bromide hydrate (CPB, 98%, Alfa Aesar), cyclohexane (99.4%, Chem-Labs) and 1-pentanol (99.4%, VWR) were used as template, solvent and co-solvent, respectively. Methylaluminoxane (PMAO-IP 7wt.% in toluene, Akzo Nobel) was used as co-catalyst for preparation of the solid activator. Zirconocene dichloride (Cp_2ZrCl_2, $Cp=\eta^5$-C_5H_5, Aldrich) was used as metallocene catalyst and tri*iso*butylaluminum (TIBA, $[(CH_3)_2CHCH_2]_3Al$, Aldrich) was employed as a scavenger in the ethylene polymerization reactions. Ethylene and nitrogen (Air Liquide) were purified through adsorption columns containing a mixture of 4A and 13X molecular sieves. Toluene (VWR) was dried by refluxing over metallic sodium under nitrogen and using benzophenone as an indicator. The other materials were used without further purification. All sensitive reactants and materials were handled under nitrogen using standard inert atmosphere techniques.

2.2. Dendrimeric silica nanospheres (DS) synthesis and characterization

The synthesis procedure used was described in a previous work[23]. Briefly, CPB (3g, 0.0078 mol) and urea (1.8 g, 0.03 mol) are dissolved in deionized water (90 mL). Separately, 1-pentanol (1.5 mL) and TEOS (7.5 g, 0.036 mol) are dissolved in cyclohexane (90 mL). The two solutions are stirred separately to ensure homogenization. The organic solution is added to the aqueous solution under vigorous stirring and the resulting mixture is further stirred for 30 minutes at room temperature. The micro-emulsion formed is finally treated at 120°C with microwave (MW) radiation for 60 minutes in Teflon autoclave vessels (MARS-5 oven, 600 W maximum power). The DS material is separated by centrifugation and washed twice with a 1:1 water and acetone solution. The resulting material is air-dried for 24 hours and after calcined at 650 °C under air for 8 hours. The characterization of the support was also performed as previously described[23], by means of nitrogen sorption measurements and morphology assessment through transmission electron microscopy.

2.3. Support Pretreatment

A batch of DS was treated at 200°C under primary vacuum for 90 minutes to remove the adsorbed water.

2.4. Nanocomposite preparation methods

2.4.1. DS-SA method

Approximately 500 mg of dry support were weighed and stored in a degassed Schlenk tube. Toluene was added with a ratio of 25 mL per gram of support and vigorously stirred. MAO was added to the suspension to achieve a surface Al loading of 3 mmol/g and vigorously stirred for 16 hours at room temperature, shielded from ambient light. The DS supported MAO suspension is then stored in a Schlenk tube and directly used in the polymerization procedure.

2.4.2. DS-MAO method

The first step of this procedure is the same pretreatment of the DS with MAO just commented, albeit with an Al loading of 4 mmol/g instead of 3 mmol/g. Later, the toluene was removed under vacuum until a light and dry powder was obtained. The dry powder was re-suspended in toluene with a ratio of 29 mL per gram of support and a toluene solution of zirconocene dichloride was prepared and added to achieve a final Zr loading of 35 µmol per gram of support. After a contact time of 4 hours, the final catalyst was stored in the Schlenk tube. Prior to its use in the ethylene polymerization, a supernatant test is conducted to confirm total immobilization.

2.5. Ethylene Polymerization

The polymerization reactor consists of a 250 mL bottle for pressure reactions (WilmadLabGlass LG-3921) with crown cap, gasket and magnetic stirrer. This reactor was placed in a water bath. Ethylene consumption rate was measured using two mass flow controllers (Hastings Instruments HFC-202 and Alicat Scientific 16 Series) and recorded in a personal computer with data acquisition hardware and software (a ComputerBoards CIO-DAS08/Jr-A0 interface card with Labtech DataLab software). Ethylene pressure was measured with a digital manometer (AirLiquide M2500), being also recorded.

The reactor was purged with vacuum/N_2 and loaded with enough toluene to match a total volume of 50 mL when polymerization was started. Nitrogen was then replaced by ethylene by means of 5 vacuum/ethylene cycles and afterwards waiting for the ethylene consumption to stabilize. At this point, the procedure changes according to the preparation method employed to prepare the catalytic system.

If the DS-SA method is applied, there is an initial addition of 1.0 mL of a 0.1 M TIBA solution to act as scavenger, followed by the addition of the appropriate volume of DS supported MAO

activator and finally the addition of a Cp_2ZrCl_2 toluene solution corresponding to 1.9 $x10^{-6}$ mol of Zr. No external MAO solution is added in this procedure.

The DS-MAO method consists in the addition of the appropriate amount of external MAO solution to achieve an Al/Zr ratio of 1500 in the polymerization medium, followed by the addition of a vigorously stirred suspension containing the zirconocene catalyst supported onto MAO pretreated DS, in order to achieve the desired support amount.

The polymerizations take place at 25 °C and 1.1 bar of ethylene. Temperature, pressure, and ethylene mass flow data are monitored during the reaction in real-time and automatically recorded. The ethylene mass flow is converted to ethylene consumption and polymerization activity calculated in $kg_{PE}/mol_{Zr}h$. The kinetic profiles correspond to ethylene consumption versus time, which after integration yields a value of average activity that is compared with the value obtained by considering the mass of recovered polymer. The reaction is stopped either at the end of 30 minutes or when the consumption of ethylene reaches approximately 2 grams, in order to avoid severe mass transfer limitations occurring after this point. After the reaction, possible solubilized polymer is precipitated over 5% HCl acidified methanol, filtered and washed twice using methanol before drying. The supernatant or clarified liquid test was followed as previously described for the DS-MAO method, in order to assess whether the catalyst was totally immobilized on the support surface.

2.6. Film preparation

Powders obtained from ethylene polymerizations are processed into thick films (of around 200 µm) by compression molding, using a Collin press. The powder is first heated up to 170°C for 2 minutes without applying any pressure in order to properly melt the polymeric matrix. Later, a pressure of approximately 2 MPa is imposed during 3 minutes at 170°C. Then, a cooling treatment is applied, which consists of a relatively fast cooling (around 80 °C/min) from the

polymer melt to room temperature between plates of the press refrigerated with cold water, keeping pressure constant at 2 MPa along this treatment.

2.7. Polymer molar mass characterization

Polymer average molar mass and dispersity were obtained through high temperature size exclusion chromatography (HT-SEC) measurements, employing a Malvern Instruments Viscotek system outfitted with three Polefin 300mm x 8 mm I.D. columns from Polymer Standards Service with corresponding porosities of 100 Å, 100,000 Å and 1,000,000 Å. 1,2,4-trichlorobenzene (TCB) was used as an eluent at a 1 ml min^{-1} flow rate and a temperature of 150 °C. 2,6-di(*tert*-butyl)-4-methylphenol was used as an eluent stabilizer under a 200 mg/L concentration. The polymers were dissolved in TCB at an approximate concentration of 1 mg/mL and 200 µL injections were performed. Online detection was performed by means of a differential refractive index detector, a viscosity detector and a dual light scattering detector (RALS and LALS) for accurate measurements. OmniSEC version 5.12 was used to calculate the polymer properties.

2.8. Morphological characterization

SEM micrographs were obtained on a Zeiss Merlin Compact equipment coupled with an Oxford EDX detector. Polymer films prepared from ethylene polymerization were fixed onto the sample holder and subjected to a carbon coating procedure prior to inserting the samples into the microscope to analyze their morphological characteristics.

2.9. Thermal stability

Thermogravimetric analysis (TGA) was performed in a Q500 model TA instruments thermobalance under oxidative and inert atmospheres. Experiments were performed from 50 to 800 °C at a heating rate of 10 °C/min. These measurements allow evaluating differences in

the degradation processes and assessing the actual amount of inorganic filler in the final composites.

2.10. Structural characterization

Wide angle X-Ray Diffraction (WAXD) patterns were recorded at room temperature in the reflection mode to examine the crystalline structure of the polymeric matrix by using a Bruker D8 Advance diffractometer provided with a PSD Vantec detector (from Bruker, Madison, Wisconsin). Cu Kα radiation (λ=0.15418 nm) was used, operating at 40 kV and 40 mA. The parallel beam optics was adjusted by a parabolic Göbel mirror with horizontal grazing incidence Soller slit of 0.12° and LiF monochromator. The equipment was calibrated with different standards. A step scanning mode was employed for the detector. The diffraction scans were collected with a 2θ step of 0.024° and 0.2 s per step.

2.11. Phase transitions

Analyses were carried out by differential scanning calorimetry (DSC) in a TA Instruments Q100 calorimeter connected to a cooling system and calibrated with different standards. Sample weights ranged from 5 to 7.5 mg. A temperature interval from -40 to 160 $^{\circ}$C was chosen and a 10 $^{\circ}$C/min heating rate was employed. A 290 J/g value was used for the enthalpy of fusion of a perfectly crystalline polyethylene[25,26].

2.12. Mechanical behavior

Nominal stress-strain tests were performed at a temperature of 25 $^{\circ}$C and a stretching rate of 10 mm/min in an MTS Q-Test Elite dynamometer with a load-cell of 100 N. Strips for these experiments were punched out from the polymer films. The dimensions of strips were 10 mm long, 1.9 mm wide and around 0.20 mm thick. At least, three different strips were stretched until fracture for a given specimen to assess the measurement accuracy of the different parameters.

3. Results and discussion

3.1.1. Preparation of the nanocomposites

The synthesis of DS reference batch and its characterization was described in detail in a previous article [23]. Figure 1 shows the TEM micrographs obtained for the pristine siliceous DS, confirming its dendrimer-like morphology and emphasizing its unique porosity, made up of the space between the growing silica fibers. The microscopy observations show nanospheres with sizes ranging from 100 to 600 nm and nitrogen sorption measurements yielded a BET surface area of 370 m^2/g and a total pore volume of 0.7 cm^3/g. For illustration, nitrogen sorption isotherm of the DS material is also presented in Figure S1 of the Supporting Information.

Regarding the nanocomposites synthesized by *in situ* polymerization, *Table 1* lists the different high density polyethylene (HDPE) materials that incorporate distinct contents in DS nanoparticles prepared by the two methodologies. Some of their features – namely, the filler content and the polymer molar mass – are reported together with the corresponding synthesis conditions used. Nanocomposites samples are named by the synthetic route used during *in situ* polymerization either DS-MAO or DS-SA followed by Nx where *N* means that is a nanocomposite and *x* stands for the DS nanoparticles weight amount determined by TGA. Polymerization time was carefully controlled to achieve nanocomposites with inorganic filler contents varying from 5 wt.% to about 20 wt.%. An additional pristine HDPE was prepared by homogeneous polymerization with the catalyst in solution, in absence of DS nanoparticles.

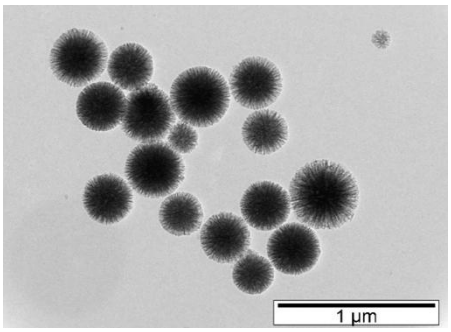

Figure 1 - TEM micrograph at two different magnifications of the DS nanospheres used in a double role: as catalytic support and as filler.

Table 1 - Polymerization conditions for the synthesis of different polyethylene nanocomposites.

Nanocomposite	Cp_2ZrCl_2 loading (µmol/g)	Filler amount (mg)	n_{Zr} (µmol)	Al/Zr	Total yield (mg)	DS content (wt. %)[a]	M_w (Da)	M_w/M_n
HDPE	-	-	1.9	1500	1330	-	225,000	2.1
DS-MAO-N5[b]	35	50	1.8	ca. 1600	1070	5	515,000	2.0
DS-MAO-N7[b]		100	3.5		1240	7	421,000	2.5
DS-MAO-N16[b]		200	7.0		1220	16	336,000	2.6
DS-MAO-N24[b]		300	10.5		1240	24	176,000	2.2
DS-SA-N5[c]	-	50	1.9	80	1000	5	423,000	2.3
DS-SA-N9[c]		100		160	1210	9	281,000	2.4
DS-SA-N15[c]		200		320	1310	15	205,000	2.7
DS-SA-N21[c]		300		470	1300	21	224,000	2.1

[a]Determined by TGA. [b] - mmol Al/g of DS. [c] 3 mmol Al/g of DS

Weight average molar masses (M_w) and dispersity (M_w/M_n) are very important molecular characteristics for all the nanocomposites. The results listed in *Table 1* show that M_w values are higher than 200,000 Da for all the materials except for the sample DS-MAO-N24, which exhibits slightly lower values. These molar mass values suggest that a suitable final mechanical performance might be expected from all of them. Additionally, it is important to indicate that, independently of the preparation method, an increase of the filler content in the nanocomposite is accompanied by a decrease in average molar mass to values closer to that exhibited by the reference HDPE. Moreover, it should be noted that within each methodology, the incorporation of higher support amounts to the reaction medium, necessarily turns out in a larger amount of Al, from MAO, which would increase the probability of chain transfer to the aluminum [24]. Accordingly, chains of shorter length would be attained at the end of those polymerizations [27] containing high amount of catalyst carrier.

Comparing the DS-MAO and DS-SA methodologies, the results show that the nanocomposites prepared through the latter present lower values of average molar mass, especially when low

filler contents are considered. It may be suggested that the inherent features to the DS-SA procedure probably result in active species that are somewhat weakly bound to the support surface and thus, the support steric protection effect, preventing β-hydride transfer, might be not as effective as for the DS-MAO procedure [24].

3.1.2. Dispersion of dendrimeric silica nanospheres

A crucial parameter affecting the ultimate performance of polymeric nanocomposite materials is the nature of filler-filler and polymer-filler interactions and their effect on the dispersion of the filler within the final nanocomposite. Dispersion is expected to be generally hindered when filler content is increased, especially when dealing with a hydrophobic polymer and a hydrophilic inorganic component. This results in a tendency to form particle agglomerates, which in turn may lead to the loss of mechanical properties in the final material [28].

Figure 2 and *Figure S2* of the Supporting Information present SEM micrographs, at 5000 and 1000 magnifications, respectively, comparing nanocomposites with low and high DS filler contents obtained from the two synthetic approaches used (*i.e.*, DS-MAO-N7 and DS-MAO-N24 as well as DS-SA -N9 and DS-SA -N21) in order to assess their dispersion associated with either the distinct incorporation amount at a given methodology or similar content at each synthetic protocol employed.

The results show important differences between all the samples, independently of the magnification. Firstly, the increase in DS content in specimens achieved at a specific approach, comparison of pictures (a) and (b) or (c) and (d), suggests that the particles tend to locate in closer vicinity as their amount is enlarged within the HDPE matrix. Presence of large particle aggregates is not, however, seen in the micrographs. On the other hand, comparison for similar DS contents at the two synthetic routes, *i.e.* pictures (a) and (c) or (b) and (d), seems to suggest that the particle dispersion is not the same but dependent on the preparation procedure. In fact, the difference between the DS-MAO and DS-SA samples is quite clear. The SEM micrographs related to samples DS-MAO-N7 and DS-MAO-N24 show darker regions that

correspond to the HDPE matrix and lighter regions constituted by a higher concentration of the DS nanospheres, indicating that a relatively heterogeneous distribution of silica nanospheres is exhibited by the nanocomposites. By contrast, the micrographs of samples DS-SA -N9 and DS-SA -N21 show a much more homogeneous distribution of the DS particles, with rather uniformly dispersed nanospheres inside the HDPE matrix.

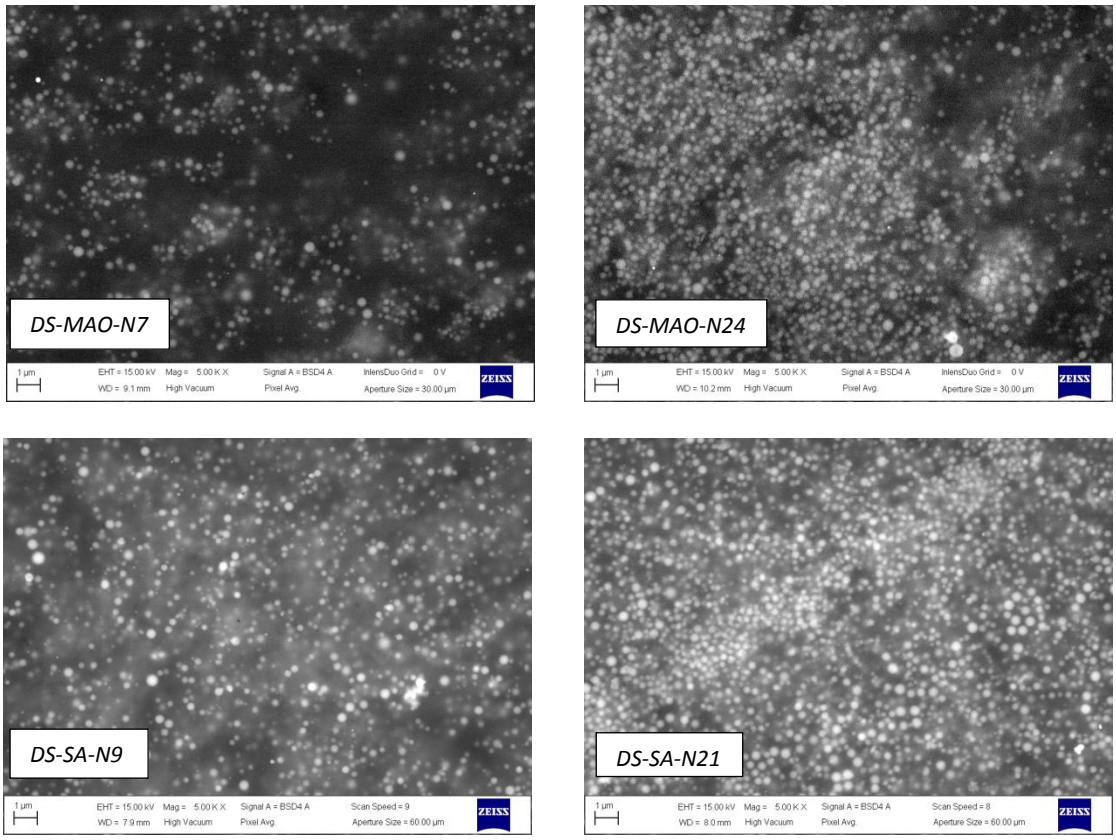

Figure 2 - SEM micrographs at 5000 times magnification of samples DS-MAO-N7, DS-MAO-N24, DS-SA-N9 and DS-SA-N21, showing the dispersion of DS nanospheres along the axial direction of the nanocomposite film.

A better dispersion of the DS filler involves an enlarged available surface area for contact between the two components, HDPE matrix and DS nanoparticles. These features could lead to a better reinforcement effect of those DS nanospheres within the HDPE in the DS-SA-Nx nanocomposites. However, it is worth noting that the pictures characterize the filler dispersion along the axial direction of the film and, as such, it is interesting to look at the dispersion along a cross-section. Thus, *Figure 3* shows those cross-section images of DS nanospheres dispersion

acquired on cryofractured specimens, evaluating again these two variables: nanofiller content and preparation method.

Comparison of samples DS-MAO-N7 (a) and DS-SA-N9 (c) shows some differences, the nanospheres in the former appear to be concentrated on the center part of the cross-section, as opposed to sample DS-SA-N9, where the DS nanoparticles appear to be dispersed across the entire section. It is interesting to highlight that the imprints left by the nanospheres in the cryofracture can be seen in the images, which occur during the separation procedure into the two halves of the film. At the highest nanosphere content, the difference in the DS dispersion between the specimens prepared by the two methods is even more evident, as also was deduced from *Figure 2* and *Figure S2* of Supporting Information. The sample DS-SA-N21 clearly presents DS nanospheres better dispersed than the sample DS-MAO-N24, as observed in the difference between the lighter and darker regions in the latter.

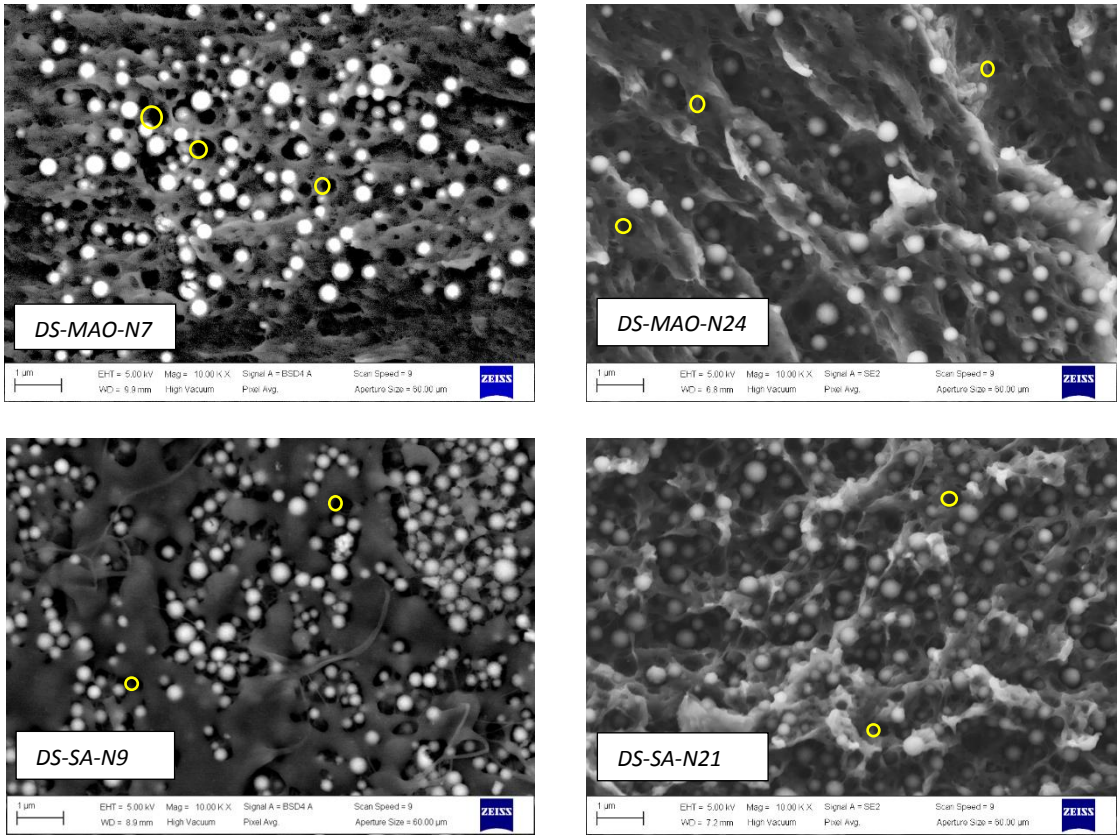

Figure 3 - SEM micrographs at 10000 times magnification of samples DS-MAO-N7, DS-MAO-N24, DS-SA-N9 and DS-SA-N21, showing the dispersion of DS nanospheres along the cross-section of the nanocomposite films.

An EDX elemental mapping of the elements across a wider surface of the cross-section has been performed to get a deeper knowledge of DS nanospheres distribution within HDPE matrix. *Figure S3* of the Supporting Information shows the acquired SEM micrograph for sample DS-MAO-N7 and the individual elemental maps of Si, O, C and Al, which are afterwards superimposed to generate a composite image. The results show the expected elemental maps, which show an abundance of carbon, with precise Si and O maps pointing out the positions of the DS nanoparticles. Additionally, the composite image reflects the abundance of C and Si/O in the image. As a simplification, further comparisons between the samples will be made resorting to the SEM micrograph and a composite image, generated from the overlapping of the different elemental maps.

Figures S4 and *S5* of Supporting Information show the SEM-EDX micrographs at 5000 times magnification for samples DS-MAO-N7 and DS-MAO-N24 in the former, and DS-SA-N9 and DS-SA-N21 in the latest, showing the dispersion of DS nanospheres along the cross-section of the cryofractured nanocomposite films. The plots on the right are recorded through EDX elemental mapping on the acquired image. These results corroborate those observed in *Figure 2*. The distribution of the DS nanospheres is more homogeneous in samples DS-SA-N9 and DS-SA-N21 (both in the film surface and the cross-section) than those incorporated into nanocomposites DS-MAO-N7 and DS-MAO-N24. The samples prepared by the DS-MAO method present areas with mainly carbon (in red) and others with mainly silicon (in green), while those prepared by the DS-SA approach present a much more homogeneous distribution.

3.1.3. Thermal stability

Knowledge of the decomposition behavior in these nanocomposites achieved by *in situ* polymerization through two different methods is a critical factor in discerning potential applications for these materials. Presence of mesoporous silica particles inside a polymeric

matrix has been described to exert, sometimes, a catalytic role in the degradation process of polymers [29–33]. Accordingly, it is interesting to study the effect of these DS nanoparticles in HDPE thermal degradation. Furthermore, the bulk DS content can be determined from these experiments once the polymer is fully decomposed.

Figure 4 shows the thermogravimetric curves for all the HDPE nanocomposites synthesized with DS nanospheres attained under two different environments. Important differences are observed in the materials depending on whether they are degraded under an oxidative or an inert atmosphere. Thus, several stages are noticeable in the former from 200 to 600 °C while a single step is seen under inert conditions in the same temperature interval. This thermal inert decomposition of pristine HDPE has been shown to take place via a scission mechanism that occurs randomly in the polymeric chain, turning out in several chain fragments of different lengths. The mechanism includes the formation of free radicals along the backbone of the macrochain, which then split the chains into a fragment with a terminal unsaturation and another one with a terminal radical that result in terminal dienes, alkenes or alkanes due to further hydrogen chain transfer reactions. The mechanism under oxidative conditions starts with the same formation of alkyl radicals, which then react with the available oxygen to yield hydroperoxides that further form alkoxyl radicals. These alkoxyl radicals easily react with the polyethylene backbone, abstracting hydrogen atoms at random and resulting in different carbonyl species [33].

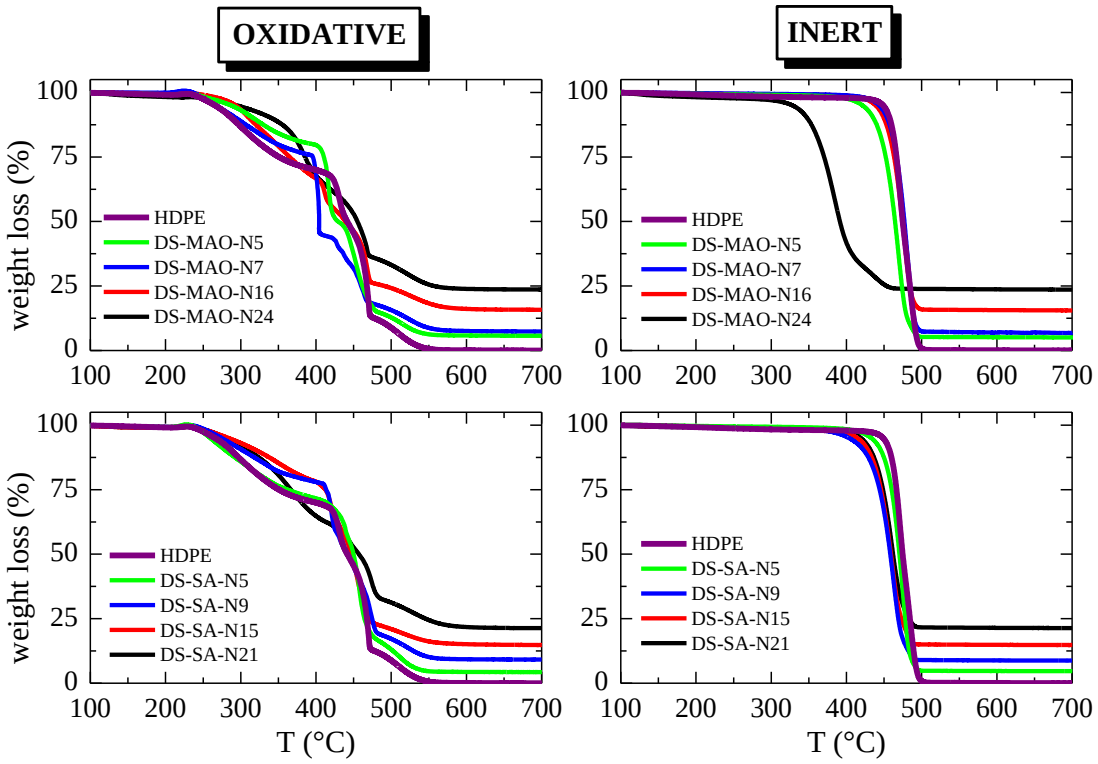

Figure 4 - Weight loss curves as function of temperature for DS-MAO and DS-SA nanocomposites under oxidative and inert atmospheres. HDPE was added as a reference.

Concerning the decomposition under an inert atmosphere, the addition of DS nanospheres causes a decrease in the temperature needed to begin decomposition regardless of the silica content. Moreover, the nanocomposites produced through the DS-SA procedure present slightly lower temperatures at the beginning of degradation than their DS-MAO counterparts, for intermediate silica content. Thus, DS nanospheres appear to have an effect on the low temperature range, which is expected as the decomposition takes place due to a combined contribution of thermal radical mechanisms and catalytic ones. As temperature raises the contribution of the thermal mechanisms increases and the effect of adding nanoparticles is diluted. Thus, the catalytic contribution of the nanoparticles is more noticeable during decomposition at lower temperatures.

When considering the polymer decomposition under oxidative conditions, the addition of DS appears to lead to an increase in the temperature needed to begin decomposition in the nanocomposites produced through the DS-MAO procedure. The same general trend applies

for nanocomposites produced through the DS-SA methodology. Furthermore, regardless of preparation procedure, a significant increase in the starting decomposition temperature is observed at high contents in silica nanospheres, as displayed in *Table 2* and *Figure 4*.

Regarding the final weight content left, which corresponds to the filler content in the final nanocomposites, results derived from oxidative or inert atmospheres do not vary significantly, fact that can be considered as other indication of homogeneity in terms of the DS nanospheres content at a given material.

Table 2 - Thermogravimetric analysis results of the prepared nanocomposites and reference pristine polyethylene. Bulk DS filler content and decomposition temperatures at specific weight loss values of 5, 20 and 50% under inert and oxidative atmospheres.

Sample	DS content (wt.%)[a]	Oxidative atmosphere			Inert atmosphere		
		$T_{5\%}$ (°C)	$T_{20\%}$ (°C)	$T_{50\%}$ (°C)	$T_{5\%}$ (°C)	$T_{20\%}$ (°C)	$T_{50\%}$ (°C)
HDPE	0	267	330	445	450	465	475
DS-MAO-N5	5	287	395	429	421	448	465
DS-MAO-N7	7	267	348	404	444	464	477
DS-MAO-N16	16	293	347	439	439	460	474
DS-MAO-N24	24	294	377	455	328	365	391
DS-SA-N5	5	260	329	450	433	457	470
DS-SA-N9	9	274	372	442	404	439	458
DS-SA-N15	15	284	383	446	414	442	459
DS-SA-N21	21	281	352	457	419	445	462

[a]Averaged between the weight content estimated under oxidative and inert atmospheres.

3.1.4. Structural characterization and thermal transitions

Figure 5 shows the WAXS diffraction profiles exhibited at room temperature by the various nanocomposite films with different DS content sand that for the pristine HDPE polymerized with the catalyst in homogeneous conditions, used as a reference.

Polyethylene is known to develop an orthorhombic lattice when crystallized under common processing conditions. This cell displays two main X-rays reflections[34,35], the (110) and (200), as seen in Figure 5. Location of these two diffractions remains rather unchanged

independently of the absence or presence of DS and its content as well as of the synthesis protocol used during polymerization.

Crystallinity degree, f_c^{WAXS}, can be estimated from these patterns by a previous subtraction of the weighted contribution of DS to the diffractogram of the nanocomposite, and further deconvolution of the resulting polyethylene profile into the different crystalline and amorphous contributions. The crystalline fraction is then derived from the ratio between the area of the crystalline reflections and the total area of the deconvoluted peaks. The calculated f_c^{WAXS} values are listed in *Table 3*.

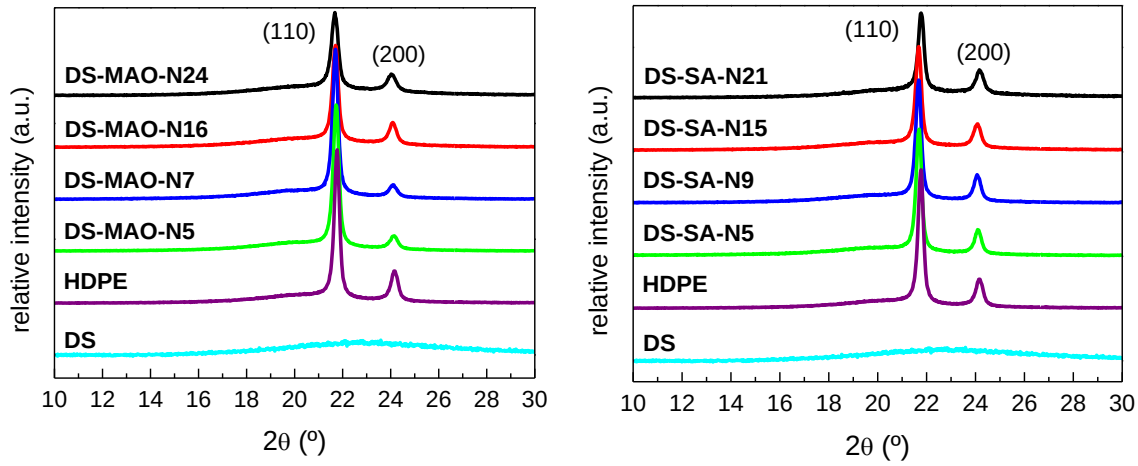

Figure 5 - WAXS profiles acquired at room temperature for the DS nanofiller, reference pristine HDPE, DS-MAO nanocomposites (left) and DS-SA nanocomposites (right).

Table 3 - DS content achieved from thermogravimetric analysis (TGA), normalized crystallinity to the actual polymer amount in each nanocomposite obtained from wide angle x-ray scattering (WAXS) (f_c^{WAXS}) as well as location of the different transitions: first melting (T_m^{F1}), crystallization (T_c) and second melting (T_m^{F2}) processes and their corresponding crystallinity degrees (f_c^{F1}, f_c^{C} and f_c^{F2}, respectively).

Sample	DS content (wt %)	f_c^{WAXS}	f_c^{F1}	T_m^{F1} (°C)	f_c^{C}	T_c (°C)	f_c^{F2}	T_m^{F2} (°C)
HDPE	0	0.58	0.56	131.0	0.60	118.0	0.60	132.5
DS-MAO-N5	5	0.57	0.55	130.5	0.59	119.0	0.59	132.5
DS-MAO-N7	7	0.57	0.55	130.5	0.59	119.5	0.59	133.5
DS-MAO-N16	16	0.53	0.52	130.0	0.56	119.5	0.56	131.5
DS-MAO-N24	24	0.53	0.52	125.5	0.55	117.0	0.55	127.5
DS-SA-N5	5	0.58	0.59	131.5	0.63	119.0	0.63	133.5

DS-SA-N9	9	0.58	0.62	131.0	0.64	119.5	0.64	133.5
DS-SA-N15	15	0.58	0.62	131.0	0.65	119.5	0.65	133.0
DS-SA-N21	21	0.58	0.63	131.5	0.66	119.5	0.66	133.5

Two different trends are observed in the variation of crystallinity f_c^{WAXS} with the DS content depending on the synthetic approach used. Those prepared by the DS-SA methodology remain constant as increasing silica amount and the values are similar to that exhibited by the neat HDPE while crystallinity degree decreases with DS content in the specimens polymerized under the DS-MAO conditions. In spite of these two tendencies, differences are not too significant.

Figure 6 shows the DSC curves corresponding to the first heating runs and subsequent cooling cycles for the different DS nanocomposites. The curves are offset to facilitate comparison of melting and crystallization temperatures as well as differences in the shape of the curves. Data derived from these DSC curves depicted in Figure 6, in addition to those achieved from the second heating run represented in Figure S6 of Supporting Information,- are listed in *Table 3* regarding DSC crystallinity for first melting (f_c^{F1}), crystallization (f_c^{C}) and second melting (f_c^{F2}), as well as the respective melting and crystallization temperatures (T_m^{F1}, $T_c$and T_m^{F2}) for the different nanocomposites, compared with those values found in the reference HDPE.

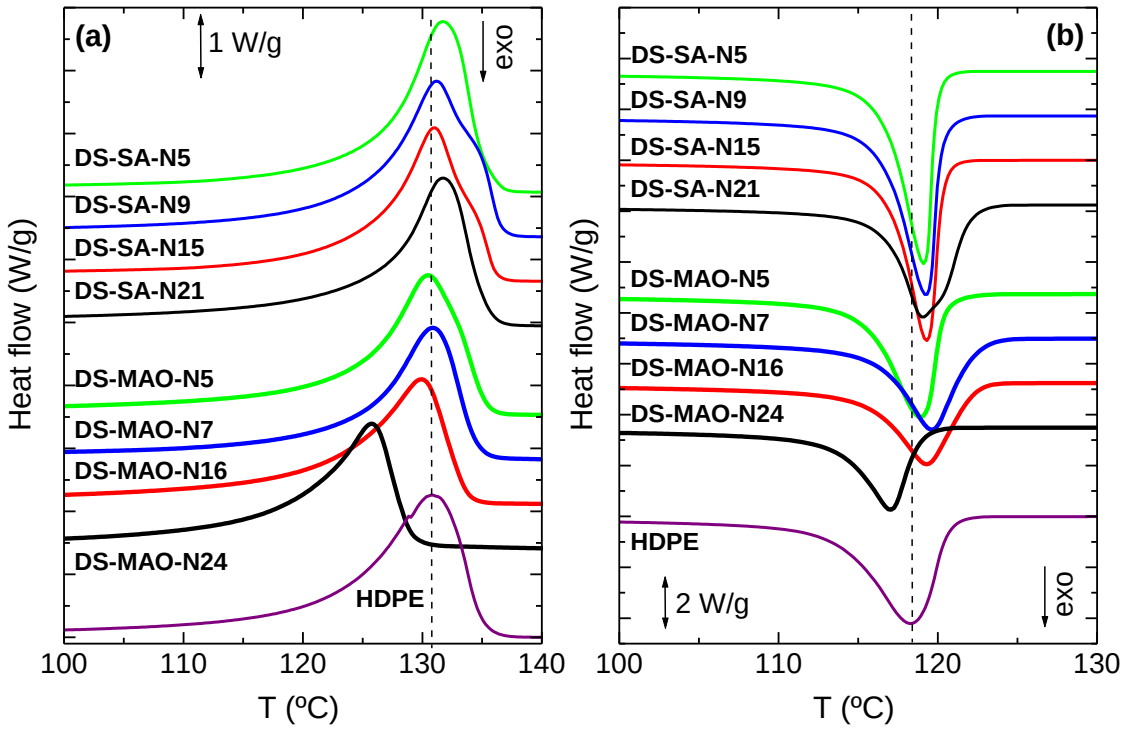

Figure 6 - DSC thermograms of the HDPE based nanocomposites with DS nanospheres for the first heating cycle (left) and cooling cycle (right) at 10 ºC/min.

At the lowest DS incorporations, DS-SA-N5, DS-SA-N9, DS-MAO-N5 and DS-MAO-N7 materials, the dependence of T_m on silica content is similar, independent of the synthetic approach and the melting temperatures are very close to that exhibited by the pristine HDPE. However, a difference is found in the shape of the DSC curves. The endotherms for the DS-MAO samples are quite uniform and unimodal while those for the DS-SA materials display a noticeable shoulder at the side of high temperature, indicating a wider distribution of the crystallite sizes. This fact could be related to differences in the interactions between polyethylene chains and surface of DS nanospheres triggered by the synthetic approach used.

The degree of crystallinity is also dependent on preparation approach. The DS-MAO materials show a lower amount of ordered chains than the DS-SA samples. Crystallinity is in the former slightly inferior while it is superior in the latest compared with the value exhibited by the neat HDPE. Correlation with the results deduced from WAXS measurements is quite good within the experimental error.

If silica content is further increased, there are no significant differences in the DS-SA materials, DS-SA-N15 and DS-SA-N21 samples, in terms of T_m and crystallinity. Then, variations of DS content do not lead to considerable changes in these DS-SA materials. A different tendency is noticeable in the DS-MAO nanocomposites. Sample DS-MAO-N16 shows a rather analogous T_m value that those found in the DS-MAO-N5 and DS-MAO-N7 specimens, but crystallinity decreases considerably as silica content increases. In the specimen DS-MAO-N24, crystallinity remains low, similar to the DS-MAO-N16 material, but the T_m value is significantly lower. This fact indicates that fewer polymeric chains were able to crystallize during processing and those crystallites were also thinner and smaller, displacing the melting process to lower temperatures.

Concerning the cooling runs in the different materials analyzed, a nucleating effect [12] is clearly observed in the polyethylene crystallization by presence of DS nanospheres in all of the nanocomposites compared with that seen in the pristine HDPE, with the exception of the DS-MAO-N24 where a hindrance is noted and, consequently, T_c is moved to slightly lower temperature. Crystallinity values deduced from crystallization are a little bit enlarged in comparison with those attained during the first melting, because now crystallization has taken place at a slower rate. Samples DS-MAO-N16 and DS-MAO-N24 develop a smaller degree of ordering than those obtained via the DS-SA protocol and also than the specimens prepared under the same conditions with lower DS contents, *i.e.*, DS-MAO-N5 and DS-MAO-N7 materials.

Crystallites attained during DSC crystallization are now more perfect than the ones achieved during initial processing of films because the DSC crystals have been generated under more favorable conditions at slower rate. Consequently, T_m^{F2} is in the second heating run at a given material higher than its value found during the first heating cycle. Again, a T_m depression is observed in the specimen DS-MAO-N24 compared with the other materials prepared by identical synthetic route or with the DS-SA materials. In these latest, T_m^{F2} remains rather

constant with the DS content, as already noted during the first melting process, and slightly superior to the value observed in the neat HDPE.

Differences in location of phase transitions (mainly the melting process), their shape and the degree of crystallinity are clearly visible for the two different methodologies. These changes are more noticeable as DS nanospheres content increases in the material. Thus, samples DS-MAO-N24 and DS-SA-N21, despite their similar silica contents show very different characteristics in terms of T_m^{F1}, T_c, T_m^{F2} and their corresponding crystallinity values (see results in *Table 3*) with the former exhibiting, basically, less and much smaller crystallites than the latter.

In order to get a deeper understanding of those differences, isothermal DSC crystallization experiments were also conducted in these two samples DS-MAO-N24 and DS-SA-N21 as well as in the neat HDPE. Thus, specimens were brought from the melt to the desired crystallization temperature, T_c, at a fast cooling rate (40 °C/min), and the heat flow evolution was registered as a function of time, as represented in the left plots (a, c and e) of *Figure 7* for HDPE, DS-MAO-N24 and DS-SA-N21. The crystallization capability of the materials was evaluated in the temperature range between 116 and 126 °C. After each isothermal crystallization, the sample was then heated from T_c to 160 °C using a heating rate of 10 °C/min, as shown in the right plots (b, d and f) of *Figure 7.*

The isothermal crystallization results show that the pristine HDPE crystallizes very slowly at 126 °C, and the ordering process speeds up as isothermal crystallization temperature T_c decreases, as clearly summarized in *Figure 8*. The lowest temperature where data are accurately observed is 119 °C, since runs performed at lower temperatures yield crystallization processes too fast to be measured. Results from the subsequent melting process show that the crystallites generated during the isothermal crystallization melt at different temperatures, these T_m shifting to higher temperatures as isothermal crystallization also increases. These results can be explained taking into account that the ordered arrangement of polyethylene

chains occurs for longer times at those high isothermal crystallization temperatures, as depicted in Figures 7 and 8. Then, macromolecules are able to crystallize under conditions more favorable than if crystallization takes place very fast. Accordingly, thicker, and more perfect crystals are developed, whose T_m values are greater than the one for thin and more defective crystallites.

A delay in the polyethylene crystallization process is clearly noticeable in sample DS-MAO-N24, when compared with the reference HDPE homopolymer. Thus, the temperature range must be modified, beginning at 123 °C instead of at 126 °C as in the reference. Similar to features described for the neat HDPE specimen, the crystallization process is homogeneous, and the different curves display a Gaussian shape. T_m values of the distinct crystallites developed under the several isothermal crystallization temperatures are considerably smaller than those exhibited by the crystals from the pristine HDPE specimen, as clearly depicted in Figure 8. These features indicate that crystals in sample DS-MAO-N24 are thinner and less perfect. Furthermore, they are developed in a significant lower amount leading to a decrease in the enthalpy involved and the subsequent crystallinity. Crystallization in the material DS-MAO-N24 is hindered compared with that process in the neat HDPE.

The polyethylene existing in DS-SA-N21 nanocomposite begins its crystallization at the highest tested temperature, 126 °C, as the reference HDPE does. Thus, contrary to the DS-MAO-N24 sample, no delay in crystallization is observed in the present case. Nevertheless, certain heterogeneity seems to be detected in the crystallization process despite this occurs in a small extent because its slowness at this temperature. That heterogeneity, which is noted as appearance of a shoulder overlapped at the side of high temperatures, becomes more evident when isothermal crystallization takes place at lower temperatures. Thus, the crystallization curves do not display a Gaussian shape. This heterogeneity was also evident in the dynamic run, as deduced from Figure 6. The crystallites generated in the isothermal runs of this nanocomposite present a T_m values considerably higher than those found for the sample

prepared via the DS-MAO procedure, as clearly noticed in Figures 8 and 9. Crystallinity is also much higher.

In summary, the isothermal results corroborate the findings obtained from the dynamic runs and highlight the main differences between the two methodologies. The DS-SA-N21 material crystallizes faster than neat HDPE and much more quickly than DS-MAO-N24, as depicted in Figure 8a. Furthermore, the polyethylene crystallites developed under isothermal conditions in the DS-SA-N21 sample are thicker than those formed in the pristine HDPE and much larger than the crystals generated in the DS-MAO-N24 specimen. Consequently, their T_ms are higher than those in HDPE and considerably greater that the ones observed in the DS-MAO-N24 material.

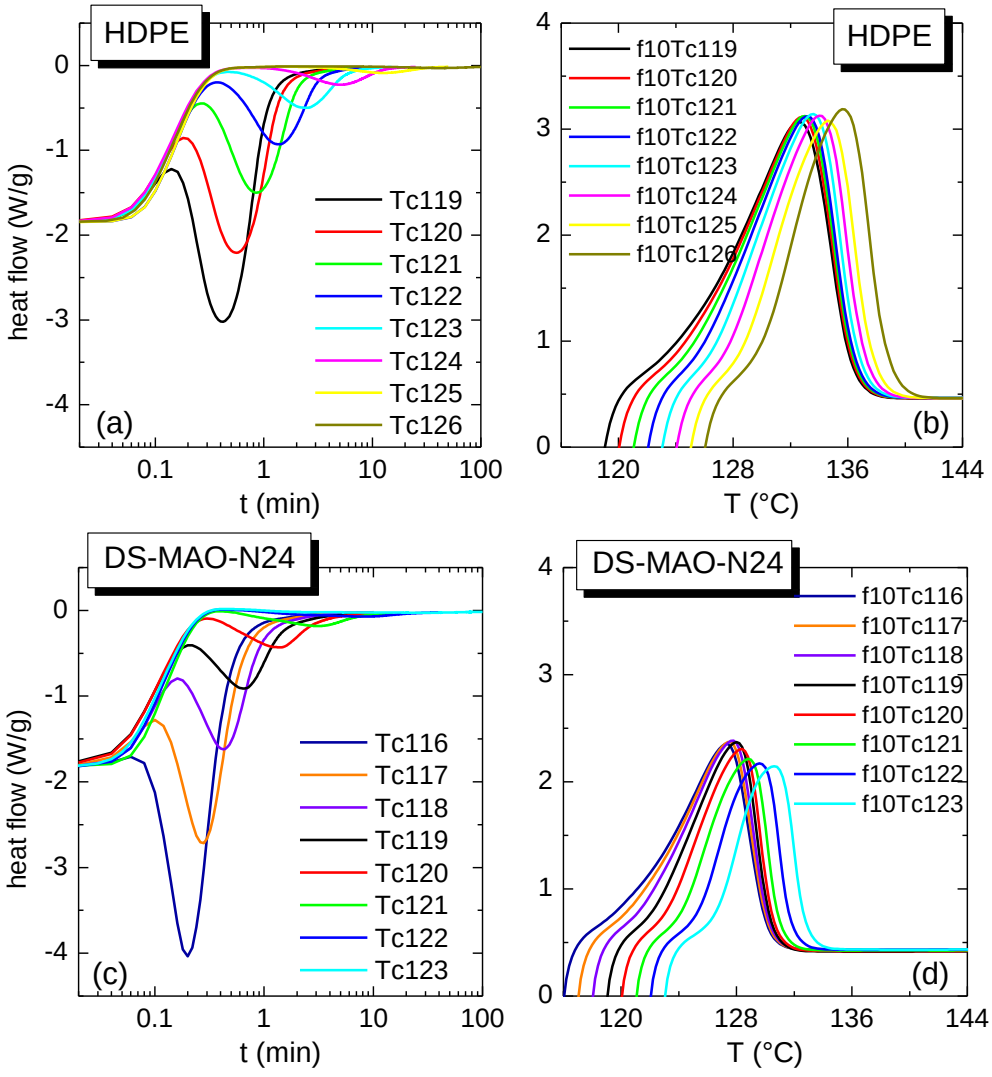

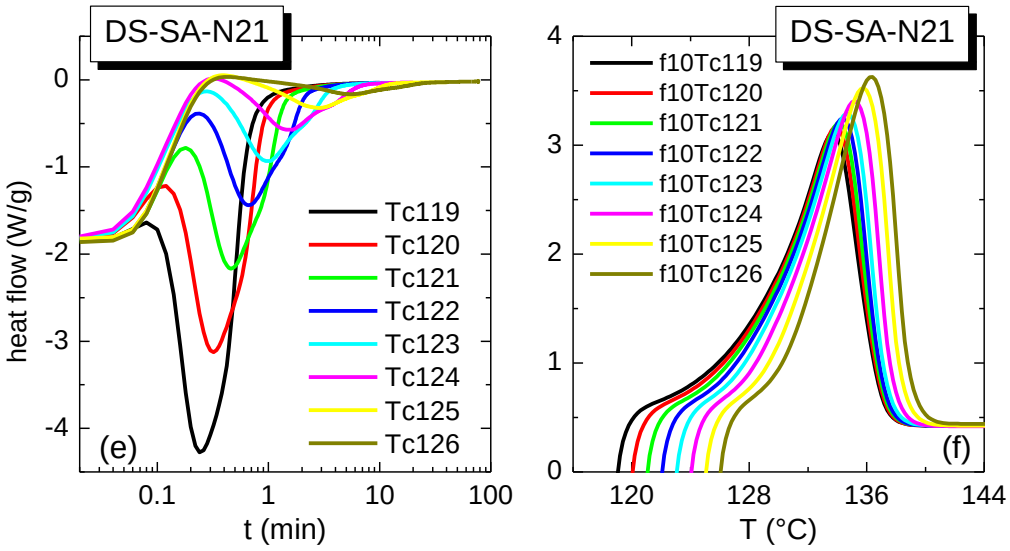

Figure 7 – Isothermal DSC crystallization (left) and subsequent heating cycle (right) thermograms obtained for the pristine HDPE (top) and the nanocomposites with the highest DS contents, the DS-MAO-N24 (middle) and DS-SA-N21 (bottom).

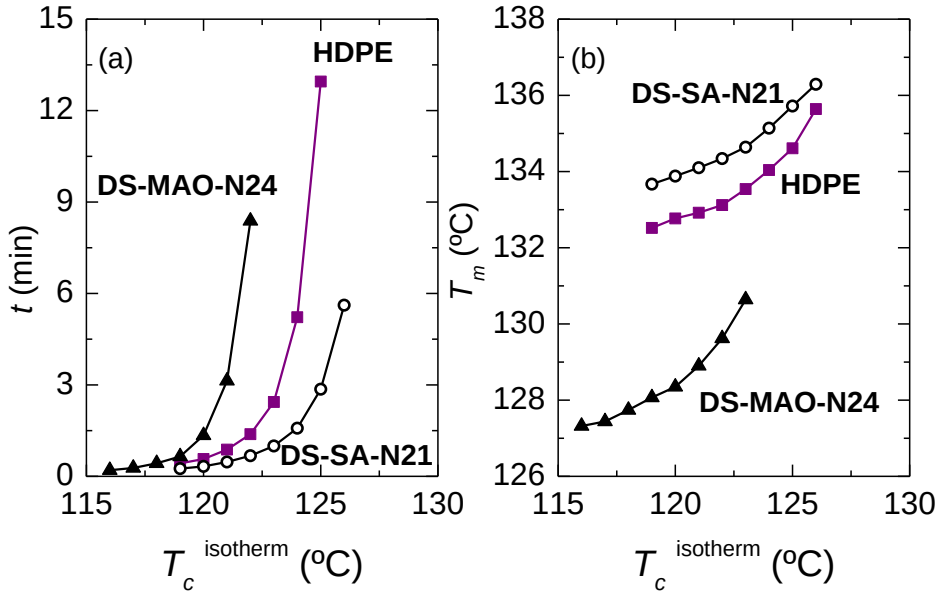

Figure 8 – Comparison of the peak crystallization time (a) and melting point (b) as a function of the temperature of isothermal crystallization for HDPE, DS-MAO-N24 and DS-SA-N21 samples.

3.1.5. Stress-strain behavior

Figure 9 represents the uniaxial deformation behavior shown by the HDPE-based materials after incorporation of DS nanospheres together with that exhibited by the neat HDPE used as reference. The average parameters deduced from the several stress-strain curves are listed in *Table 4*

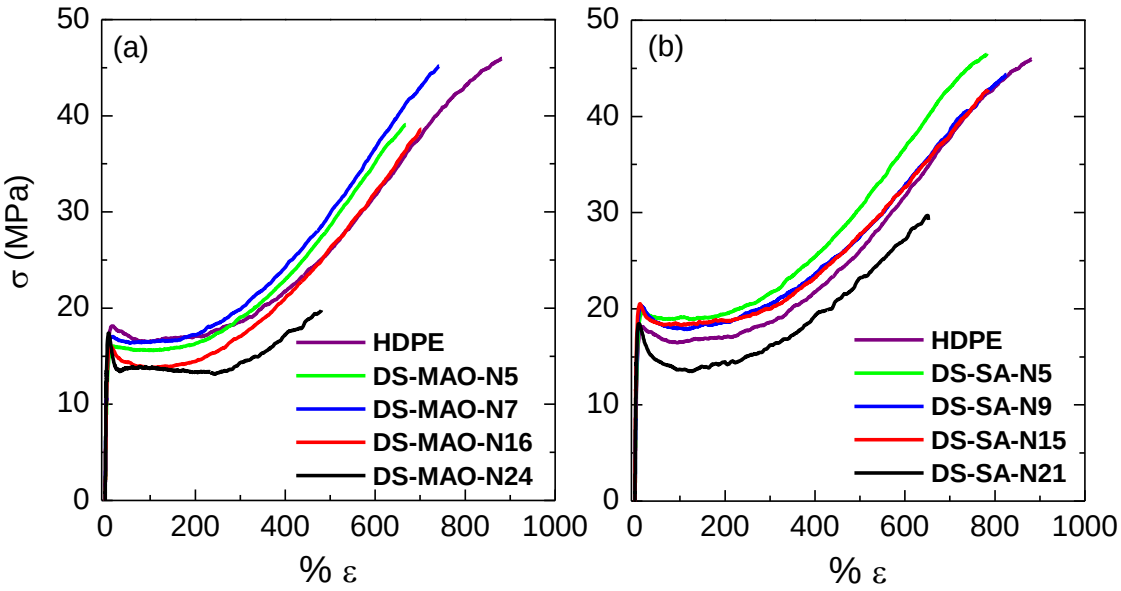

Figure 9 - Stress-strain curves for the DS-MAO (a) and DS-SA (b) nanocomposites at room temperature. Pristine HDPE is included as reference.

The engineering stress-strain curves at room temperature depicted in *Figure* represent the common behavior of ductile polymers, such as HDPE. Three regions are clearly shown in all of them: the elastic zone, where the stress rises linearly with strain up to the yielding point, which can be considered as the minimal stress required inducing a permanent deformation in the material; a narrow region where the stress is maintained relatively constant with increasing strain; and, the last zone, named as strain hardening, where stress starts to rise with strain associated with stress-induced orientation of the polymeric macrochains. This process ends with the break of the material, which is characterized by the tensile strength (σ_{break}) and elongation at break (ε_{break}).

Table 4 - Mean Young's Modulus, Yield Stress, Ultimate Stress and Elongation at break values for the DS-MAO and DS-SA nanocomposites, as well as the reference neat HDPE.

Sample	DS content (wt %)	E (MPa)	σ_Y (MPa)	σ_{break} (MPa)	ε_{break} (%)
HDPE	0	415	18.5	40.0	840
DS-MAO-N5	5	460	16.5	41.0	660
DS-MAO-N7	7	480	16.0	44.0	790
DS-MAO-N16	16	520	16.0	38.5	700
DS-MAO-N24	24	610	15.5	20.0	480
DS-SA-N5	5	550	19.5	46.0	780

DS-SA-N9	9	590	20.0	43.5	830
DS-SA-N15	15	655	20.0	44.5	870
DS-SA-N21	21	675	18.0	26.5	650

Results shown in Table 4 and *Figure* show that incorporation of DS nanospheres leads to materials stiffer than pristine HDPE and, therefore, an increase of Young´s modulus (E) is noticeable, independently of the protocol used during polymerization, compared with that exhibited by neat HDPE. This increase in rigidity becomes more pronounced as DS content rises in the nanocomposites. This feature can be ascribed to the reinforcement role that silica nanoparticles exert on the HDPE matrix, since silica is more rigid than the polymeric chains of HDPE. Nevertheless, variation of E as a function of the amount of DS nanospheres is dependent on the synthetic approach used for polymerization. Thus, E increase is rather linear in the materials prepared by the DS-MAO protocol while a dissimilar tendency is shown in those nanocomposites obtained from the DS-SA methodology. This different trend could be associated with the fact that crystallinity decreases in the former samples with DS content and their values are lower than that exhibited in HDPE. Thus, comparing with the neat HDPE, the DS is the only additional component acting as filler. In the DS-SA materials, crystallinity rises as DS amount does and their values are higher than those in HDPE existing actually two constituents acting as fillers: DS nanoparticles and HDPE crystallites. In addition to these crystallinity differences, HDPE crystallites in the DS-SA materials appear to be slightly thicker than the ones achieved by the DS-MAO strategy, since they exhibit higher melting temperatures, especially at the highest filler content. Furthermore, a better dispersion of the DS nanospheres with fewer and smaller aggregates has been found in these DS-SA specimens compared with those characteristics shown by the DS-MAO samples (see *Figure 2* and *Figure 3*). That means that there is an enlarged available surface area for contact between the two components, HDPE polymer and DS filler and, likely, a stronger matrix-filler interphase can be formed. This could improve the stress transfer between both phases and increase the

contribution of the interphase to the stiffening of the nanocomposites. All these features, the synthetic protocol together with the derived morphological and structural characteristics, make the reinforcement effect in the DS-SA materials stronger than in the DS-MAO nanocomposites.

Concerning yield stress parameter, its magnitude changes in an extent significantly less important with the increase in DS content compared with the just discussed E variation. Two opposite trends are observed depending on the used methodology. A decreasing tendency is seen in the DS-MAO samples, which is more evident at the lowest DS amount and reaches an almost plateau at the highest ones. Nevertheless, yield stress rises with DS content in the DS-SA nanocomposites up to the DS-SA-N16, showing the DS-SA-N21 a value slightly inferior to that shown by the neat HDPE. Nearly constancy in the yield stress values has been also described in nanocomposites based on isotactic polypropylene (iPP) and mesoporous SBA-15 silica [32]. Furthermore, the limit for elastic zone becomes narrower with increasing DS content and, consequently, yield strain is moved to lower deformation.

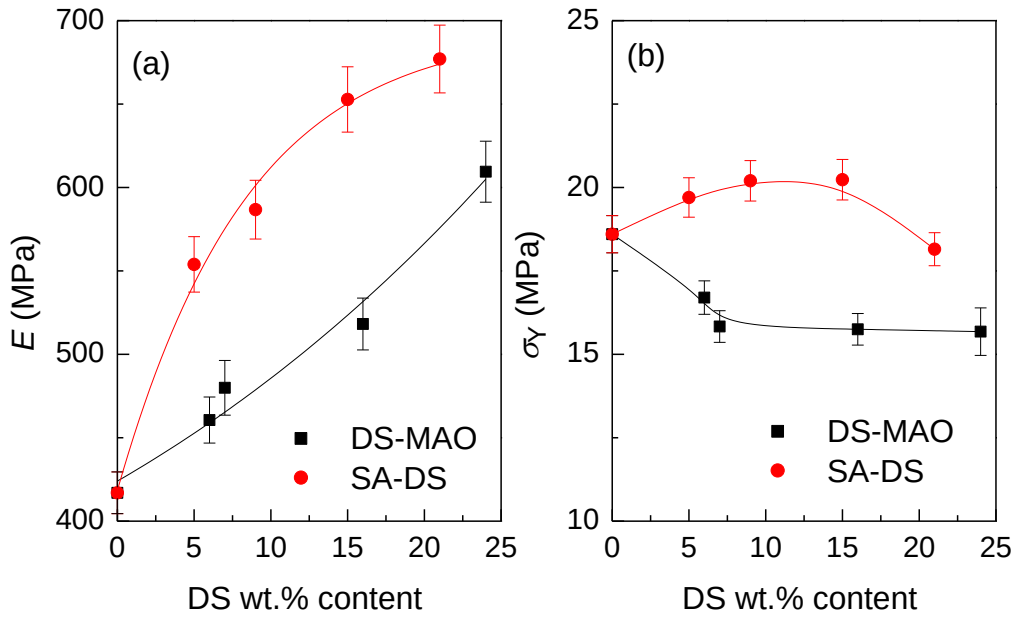

Figure 10 - Mean Young's modulus and yield stress dependence on inorganic content for the different nanocomposites and the pristine HDPE taken as reference.

All of the samples analyzed exhibit a stretching process through smooth necking formation, whose propagation occurs rapidly because of the almost elastomer-like behavior at room temperature for the HDPE matrix, regardless of the absence or presence of the inorganic component. Thus, strain hardening region starts at relatively low strain values when neck propagation ends. Level of stress in the different materials, except for DS-MAO-N25 and DS-SA-N21, the two with the highest loadings, increases from the stress plateau after yielding to the breaking from below 20 MPa to about 40 MPa in the worse cases. The high degree of deformability that these nanocomposites show can be associated with a high elastic contribution on their overall deformation process that provokes a considerable recovery after their breaking. This recovery is sensibly less in the two more rigid materials DS-MAO-N25 and DS-SA-N21, although it is still important taking into consideration their high contents.

Another very relevant aspect here is that breaking deformation in all of the nanocomposites is always superior to 450%, although relatively high contents of dendrimer-like silica have been incorporated to HDPE, as much as 24 wt.%. This is an unusual feature in (nano)composites[9,36], and even more without using compatibilizing agents, taking into account the very different chemical nature between the hydrophobic HDPE matrix and the hydrophilic DS filler. This remarkable characteristic could be associated with the preparation approaches employed. Indeed, properties are clearly better in those materials obtained from the DS-SA synthetic route, turning out the most effective approach, but even the DS-MAO procedure has allowed a good phase compatibilization and filler dispersion with absence of large particle clusters. As mentioned previously, the appropriate dispersion and lack of an important filler aggregation is one of the main advantages of manufacturing polymer nanocomposites through *in-situ* polymerization compared with other strategies. These features (good compatibilization, dispersion and absence of aggregates) were also macroscopically noticed on the aspect of films, which exhibited very nice superficial and optical characteristics. It is also worth noting that changes on the synthetic *in-situ* protocol

may be determinant to achieve improved filler dispersions at both low and high contents. The novel DS-SA methodology that we have developed [24]leads to excellent properties at polymeric matrix-filler interfaces, to a better dispersion, to a higher crystallinity and to larger crystallites than the protocol DS-MAO, contributing towards the higher overall mechanical performance.

4. Conclusions

Several HDPE nanocomposites, based on unique dendrimer like silica particles, were successfully prepared using two different methodologies, which includes an innovative approach recently reported, inspired by an *in-situ* catalyst supporting concept, DS-SA, and a more common route, DS-MAO.

Results have shown that presence of DS nanoparticles does not affect considerably the decomposition of HDPE matrix in the different nanocomposites, independently of the procedure used for their synthesis. However, a better DS dispersion and more favorable matrix-filler interactions were found for the nanocomposites prepared via the DS-SA method, when compared with DS-MAO one. Moreover, crystallinity and crystal size are also dependent on the synthetic approach used. The DS-SA nanocomposites showed higher crystallinity and T_m values. These results were corroborated by isothermal crystallization results, indicating that the DS-SA-N21 sample crystallizes much quicker than DS-MAO-N24 and that the crystallites developed in the former are much larger than the ones in the latest. Furthermore, the DS nanospheres play a nucleating effect during their crystallization independently of DS content. Accordingly, the synthetic protocol has a very important effect on the derived morphological and structural characteristics and make that DS reinforcement, turns out in the DS-SA materials stronger than in the DS-MAO nanocomposites. Consequently, Young´s modulus and yield stress are undoubtedly higher in DS-SA nanocomposites.

Another remarkable feature, common for all the hybrid materials, is to exhibit an elongation at break always higher than 450%, even at contents of dendrimer-like silica incorporated into the

corresponding HDPE higher than 20 wt.%. Thus, an excellent balance between stiffness and deformability ability is achieved in these materials. This is particularly noticeable for the DS-SA materials and namely for the highest content samples; DS-SA-N15 and DS-SA-N21, where an improvement greater than 60 % in the rigidity can be achieved when compared with the HDPE reference sample, while keeping the limit stretching ability of the nanocomposites near the pristine polymer value. In contrast, the mechanical performance of DS-MAO samples and particularly of the DS-MAO-N24 specimen is clearly weaker. In fact, the E modulus only increases ~40%, while the elongation at break shows a marked reduction, ~ 40%, when compared to the HDPE reference sample.

Summarizing, the preparation approach used to attain HDPE nanocomposites with DS nanospheres strongly affects the morphological, structural, and mechanical characteristics of the resulting materials. Although both methodologies yield nanocomposites exhibiting improved mechanical features, the DS-SA protocol indeed appears as the most effective to prepare high-performance polyolefin nanocomposites through *in-situ* polymerization. As reported in our previous publication, the high polymerization activity attained at a markedly lower activator amount, is now actually combined with a superior crystalline fraction, filler dispersion and mechanical stiffness for similar filler loadings. Furthermore, the nanocomposites retain the HDPE limit stretching ability to a surprising degree, thus confirming the high potential of the DS-SA method for the preparation of high-performance polyethylene-based nanocomposites with an excellent balance between stiffness and deformability. These materials are thus, potential candidates to be used in applications where high-performance HDPE materials are required. One possibility refers to pressure piping systems, which require materials with high stiffness and low brittleness.

Acknowledgements

The authors gratefully acknowledge the funding of this work by Fundação para a Ciência e Tecnologia (FCT), CQE-FCT 55 (UIDB/00100/2020), the FCT-CATSUS program and the PAUILF

(Project TC 04/17). D.M.Cecílio's PhD scholarship (PD/BD/114580/2016) provided by FCT is gratefully acknowledged. This work was also supported by the Agencia Estatal de Investigación (AEI, Spain) together with the European Regional Development Fund (FEDER, UE) (MAT2016-79869-C2-1-P) and by CSIC (grant number 2020AEP129). Authors are grateful to the Characterization Service at ICTP-CSIC for TGA and mechanical facilities as well as to its personnel for support.

References

[1] J.M. Campos, J.P. Lourenço, H. Cramail, M.R. Ribeiro, Nanostructured silica materials in olefin polymerisation: From catalytic behaviour to polymer characteristics, Prog. Polym. Sci. 37 (2012) 1764–1804. https://doi.org/10.1016/J.PROGPOLYMSCI.2012.02.006.

[2] J. Wang, D. Liu, Q. Li, C. Chen, Z. Chen, P. Song, J. Hao, Y. Li, S. Fakhrhoseini, M. Naebe, X. Wang, W. Lei, Lightweight, Superelastic Yet Thermoconductive Boron Nitride Nanocomposite Aerogel for Thermal Energy Regulation, ACS Nano. (2019). https://doi.org/10.1021/ACSNANO.9B02182.

[3] W. Ma, Y. Li, M. Zhang, S. Gao, J. Cui, C. Huang, G. Fu, Biomimetic Durable Multifunctional Self-Cleaning Nanofibrous Membrane with Outstanding Oil/Water Separation, Photodegradation of Organic Contaminants, and Antibacterial Performances, ACS Appl. Mater. Interfaces. 12 (2020) 34999–35010. https://doi.org/10.1021/ACSAMI.0C09059.

[4] A.M. Díez-Pascual, M. Naffakh, C. Marco, G. Ellis, M.A. Gómez-Fatou, High-performance nanocomposites based on polyetherketones, Prog. Mater. Sci. 57 (2012) 1106–1190. https://doi.org/10.1016/J.PMATSCI.2012.03.003.

[5] B.I. Oladapo, S.A. Zahedi, F.T. Omigbodun, A systematic review of polymer composite in biomedical engineering, Eur. Polym. J. 154 (2021) 110534. https://doi.org/10.1016/J.EURPOLYMJ.2021.110534.

[6] A. Kubacka, M. Ferrer, M. Fernández-García, C. Serrano, M.L. Cerrada, M. Fernández-García, Tailoring polymer–TiO2 film properties by presence of metal (Ag, Cu, Zn) species: Optimization of antimicrobial properties, Appl. Catal. B Environ. 104 (2011) 346–352. https://doi.org/10.1016/J.APCATB.2011.01.046.

[7] J.M. Martínez-Burgos, R. Benavente, E. Pérez, M.L. Cerrada, Effect of short glass fiber on structure and viscoelastic behavior of olefinic polymers synthesized with metallocene catalyst, J. Polym. Sci. Part B Polym. Phys. 41 (2003) 1244–1255. https://doi.org/10.1002/polb.10472.

[8] M.L. Cerrada, R. Benavente, E. Pérez, Crystalline Structure and Viscoelastic Behavior in Composites of a Metallocenic Ethylene-1-octene Copolymer and Glass Fiber, Macromol. Chem. Phys. 203 (2002) 718–726. https://doi.org/10.1002/1521-3935(20020301)203:4<718::AID-MACP718>3.0.CO;2-S.

[9] M.L. Cerrada, R. Benavente, E. Pérez, Effect of Short Glass Fiber on Structure and Mechanical Behavior of an Ethylene–1-Octene Copolymer, Macromol. Chem. Phys. 202 (2001) 2686–2695. https://doi.org/10.1002/1521-3935(20010901)202:13<2686::AID-MACP2686>3.0.CO;2-L.

[10] D.M. Laura, H. Keskkula, J.W. Barlow, D.R. Paul, Effect of glass fiber and maleated ethylene–propylene rubber content on tensile and impact properties of Nylon 6, Polymer (Guildf). 41 (2000) 7165–7174. https://doi.org/10.1016/S0032-3861(00)00049-

5.
[11] M.L. Cerrada, A. Bento, E. Pérez, V. Lorenzo, J.P. Lourenço, M.R. Ribeiro, Hybrid materials based on polyethylene and MCM-41 microparticles functionalized with silanes: Catalytic aspects of in situ polymerization, crystalline features and mechanical properties, Microporous Mesoporous Mater. 232 (2016) 86–96. https://doi.org/10.1016/J.MICROMESO.2016.06.011.
[12] A. Bento, J.P. Lourenço, A. Fernandes, M.L. Cerrada, M. Rosário Ribeiro, Functionalization of Mesoporous MCM-41 (Nano)particles: Preparation Methodologies, Role on Catalytic Features, and Dispersion Within Polyethylene Nanocomposites, ChemCatChem. 5 (2013) 966–976. https://doi.org/10.1002/cctc.201200639.
[13] H. Zou, S. Wu, J. Shen, Polymer/Silica Nanocomposites: Preparation, Characterization, Properties, and Applications, Chem. Rev. 108 (2008) 3893–3957. https://doi.org/10.1021/cr068035q.
[14] S. Kango, S. Kalia, A. Celli, J. Njuguna, Y. Habibi, R. Kumar, Surface modification of inorganic nanoparticles for development of organic–inorganic nanocomposites—A review, Prog. Polym. Sci. 38 (2013) 1232–1261. https://doi.org/10.1016/J.PROGPOLYMSCI.2013.02.003.
[15] S.Y. Fu, X.Q. Feng, B. Lauke, Y.W. Mai, Effects of particle size, particle/matrix interface adhesion and particle loading on mechanical properties of particulate–polymer composites, Compos. Part B Eng. 39 (2008) 933–961. https://doi.org/10.1016/J.COMPOSITESB.2008.01.002.
[16] J. M. Campos, J. Paulo Lourenço, E. Pérez, M.L. Cerrada, M.R. Ribeiro, Self-reinforced hybrid polyethylene/mcm-41 nanocomposites: In-situ polymerisation and effect of MCM-41 content on rigidity, J. Nanosci. Nanotechnol. 9 (2009) 3966–3974. https://doi.org/10.1166/jnn.2009.1298.
[17] R. Barranco-García, A.E. Ferreira, M.R. Ribeiro, V. Lorenzo, A. García-Peñas, J.M. Gómez-Elvira, E. Pérez, M.L. Cerrada, Hybrid materials obtained by in situ polymerization based on polypropylene and mesoporous SBA-15 silica particles: Catalytic aspects, crystalline details and mechanical behavior, Polymer (Guildf). 151 (2018) 218–230. https://doi.org/10.1016/j.polymer.2018.07.072.
[18] G. Armstrong, An introduction to polymer nanocomposites, Eur. J. Phys. 36 (2015) 63001. https://doi.org/10.1088/0143-0807/36/6/063001.
[19] A. Bento, J.P. Lourenço, A. Fernandes, M.R. Ribeiro, J. Arranz-Andrés, V. Lorenzo, M.L. Cerrada, Gas permeability properties of decorated MCM-41/polyethylene hybrids prepared by in-situ polymerization, J. Memb. Sci. 415–416 (2012) 702–711. https://doi.org/10.1016/J.MEMSCI.2012.05.058.
[20] M.L. Cerrada, E. Pérez, J.P. Lourenço, A. Bento, M.R. Ribeiro, Decorated MCM-41/polyethylene hybrids: Crystalline details and viscoelastic behavior, Polymer (Guildf). 54 (2013) 2611–2620. https://doi.org/10.1016/J.POLYMER.2013.03.010.
[21] W. Kaminsky, A. Funck, K. Wiemann, Nanocomposites by In Situ Polymerization of Olefins with Metallocene Catalysts, Macromol. Symp. 239 (2006) 1–6. https://doi.org/10.1002/masy.200690084.
[22] L. Wei, T. Tang, B. Huang, Synthesis and characterization of polyethylene/clay–silica nanocomposites: A montmorillonite/silica-hybrid-supported catalyst and in situ polymerization, J. Polym. Sci. Part A Polym. Chem. 42 (2004) 941–949. https://doi.org/10.1002/pola.11053.
[23] D.M. Cecílio, A. Fernandes, J.P. Lourenço, M. Rosário Ribeiro, Aluminum Containing Dendrimeric Silica Nanoparticles as Promising Metallocene Catalyst Supports for Ethylene Polymerization, ChemCatChem. 10 (2018) 3761–3769. https://doi.org/10.1002/cctc.201800534.
[24] D. Cecílio, A. Fernandes, J.P. Lourenço, T.F.L. McKenna, M. Rosário Ribeiro, Innovative route for the preparation of high-performance polyolefin materials based on unique

dendrimeric silica particles, Polym. Chem. (2021). https://doi.org/10.1039/D1PY00453K.
[25] F.A. Quinn, L. Mandelkern, Thermodynamics of Crystallization in High Polymers: Poly-(ethylene)1, J. Am. Chem. Soc. 80 (1958) 3178–3182. https://doi.org/10.1021/ja01546a003.
[26] B. Wunderlich, Macromolecular Physics, 1st ed., Elsevier, 1980. https://doi.org/https://doi.org/10.1016/C2009-0-22032-0.
[27] E. Quintanilla, F. di Lena, P. Chen, Chain transfer to aluminium in MAO-activated metallocene-catalyzed polymerization reactions, Chem. Commun. (2006) 4309–4311. https://doi.org/10.1039/B607248H.
[28] M.M. Rueda, M.-C. Auscher, R. Fulchiron, T. Périé, G. Martin, P. Sonntag, P. Cassagnau, Rheology and applications of highly filled polymers: A review of current understanding, Prog. Polym. Sci. 66 (2017) 22–53. https://doi.org/10.1016/J.PROGPOLYMSCI.2016.12.007.
[29] A. Marcilla, A. Gómez-Siurana, D. Berenguer, Study of the influence of the characteristics of different acid solids in the catalytic pyrolysis of different polymers, Appl. Catal. A Gen. 301 (2006) 222–231. https://doi.org/10.1016/J.APCATA.2005.12.018.
[30] A. Marcilla, A. Gómez-Siurana, S. Menargues, R. Ruiz-Femenia, J.C. García-Quesada, Oxidative degradation of EVA copolymers in the presence of MCM-41, J. Anal. Appl. Pyrolysis. 76 (2006) 138–143. https://doi.org/10.1016/J.JAAP.2005.10.004.
[31] M.L. Cerrada, E. Pérez, J.P. Lourenço, J.M. Campos, M. Rosário Ribeiro, Hybrid HDPE/MCM-41 nanocomposites: Crystalline structure and viscoelastic behaviour, Microporous Mesoporous Mater. 130 (2010) 215–223. https://doi.org/10.1016/j.micromeso.2009.11.009.
[32] J. Aguado, D.P. Serrano, M.D. Romero, J.M. Escola, Catalytic conversion of polyethylene into fuels over mesoporous MCM-41, Chem. Commun. (1996) 725–726. https://doi.org/10.1039/CC9960000725.
[33] F.S.M. Sinfrônio, A.G. Souza, I.M.G. Santos, V.J. Fernandes Jr., C. Novák, Z. Éhen, Influence of H-ZSM-5, Al-MCM-41 and acid hybrid ZSM-5/MCM-41 on polyethylene decomposition, J. Therm. Anal. Calorim. 85 (2006) 391–399. https://doi.org/10.1007/s10973-006-7535-0.
[34] K. Shirayama, S.-I. Kita, H. Watabe, Effects of branching on some properties of ethylene/α-olefin copolymers, Die Makromol. Chemie. 151 (1972) 97–120. https://doi.org/10.1002/macp.1972.021510108.
[35] C.W. Bunn, The crystal structure of ethylene, Trans. Faraday Soc. 40 (1944) 23–25. https://doi.org/10.1039/TF9444000023.
[36] R. Barranco-García, J.M. López-Majada, V. Lorenzo, J.M. Gómez-Elvira, E. Pérez, M.L. Cerrada, Confinement of iPP chains in the interior of SBA-15 mesostructure ascertained by gas transport properties in iPP-SBA-15 nanocomposites prepared by extrusion, J. Memb. Sci. 569 (2019) 137–148. https://doi.org/10.1016/J.MEMSCI.2018.10.009.

Table Captions

Table1 - Polymerization conditions for the synthesis of different polyethylene nanocomposites.

Table 2 - Thermogravimetric analysis results of the prepared nanocomposites and reference pristine polyethylene. Bulk DS filler content and decomposition temperatures at specific weight loss values of 5, 20 and 50% under inert and oxidative atmospheres.

Table 3 - DS content achieved from thermogravimetric analysis (TGA), normalized crystallinity to the actual polymer amount in each nanocomposite obtained from wide angle x-ray scattering (WAXS) (f_c^{WAXS}) as well as location of the different transitions: first melting (T_m^{F1}), crystallization (T_c) and second melting (T_m^{F2}) processes and their corresponding crystallinity degrees (f_c^{F1}, f_c^{C} and f_c^{F2}, respectively).

Table4 - Mean Young's Modulus, Yield Stress, Ultimate Stress and Elongation at break values for the DS-MAO and DS-SA *nanocomposites, as well as the reference neat HDPE.*

Figure Captions

Figure 1- TEM micrograph of the DS nanospheres used in a double role: as catalytic support and as filler.

Figure 1 - SEM micrographs at 5000 times magnification of samples DS-MAO-N7 (a), DS-MAO-N24 (b), DS-SA-*N9 (c) and* DS-SA-*N21 (d), showing the dispersion of DS nanospheres along the axial direction of the nanocomposite film.Figure 3 - SEM micrographs at 10000 times*

Figure 2 - SEM micrographs at 10000 times magnification of samples DS-MAO-N7 (a), DS-MAO-N24 (b), DS-SA-*N9 (c) and* DS-SA-*N21 (d), showing the dispersion of DS nanospheres along the cross-section of the nanocomposite films.*

Figure 3 - Weight loss curves as function of temperature for DS-MAO and DS-SA *nanocomposites under oxidative and inert atmospheres. HDPE was added as a reference.*

Figure 4 - WAXS profiles acquired at room temperature for the DS nanofiller, reference pristine HDPE, DS-MAO nanocomposites (left) and DS-SA *nanocomposites (right).*

Figure 5 - DSC thermograms of the HDPE based nanocomposites with DS nanospheres for the first heating cycle (left) and cooling cycle (right) at 10 ºC/min.

Figure 7 – Isothermal DSC crystallization (left) and subsequent heating cycle (right) thermograms obtained for the pristine HDPE (top) and the nanocomposites with the highest DS contents, the DS-MAO-N24 (middle) and DS-SA-*N21 (bottom).*

Figure 8 – Comparison of the peak crystallization time (a) and melting point (b) as a function of the temperature of isothermal crystallization for HDPE, DS-MAO-N24 and DS-SA-*N21 samples.*

Figure 9 - Stress-strain curves for the DS-MAO (a) and DS-SA *(b) nanocomposites at room temperature. Pristine HDPE is included as reference.*